Electronic Supplementary Material (ESI) for Materials Advances.
This journal is © The Royal Society of Chemistry 2022

Emulating Short-Term Plasticity of a Biological Synapse with a Ruthenium Complex-based Organic Mixed Ionic-Electronic Conductor

Samuel Shin[a,b], Dae Cheol Kang[a,c], Keonhee Kim[a,c], Yeonjoo Jeong[a], Jaewook Kim[a], Suyoun Lee[a], Joon Young Kwak[a], Jongkil Park[a], Gyu Weon Hwang[a], Kyeong-Seok Lee[a], Jong Keuk Park[a], Jian Li[b,*], and Inho Kim[a,*]

[a] Neuromorphic Engineering, Korea Institute of Science and Technology, Seoul 02792, South Korea

[b] Materials Science and Engineering, Arizona State University, Tempe, Arizona 85284, United States

[c] School of Electrical Engineering, Korea University, Seoul 02841, South Korea

* Corresponding authors.

E-mail addresses: jian.li@asu.edu (J. Li), inhok@kist.re.kr (I. Kim)

OMIEC Device Structure.

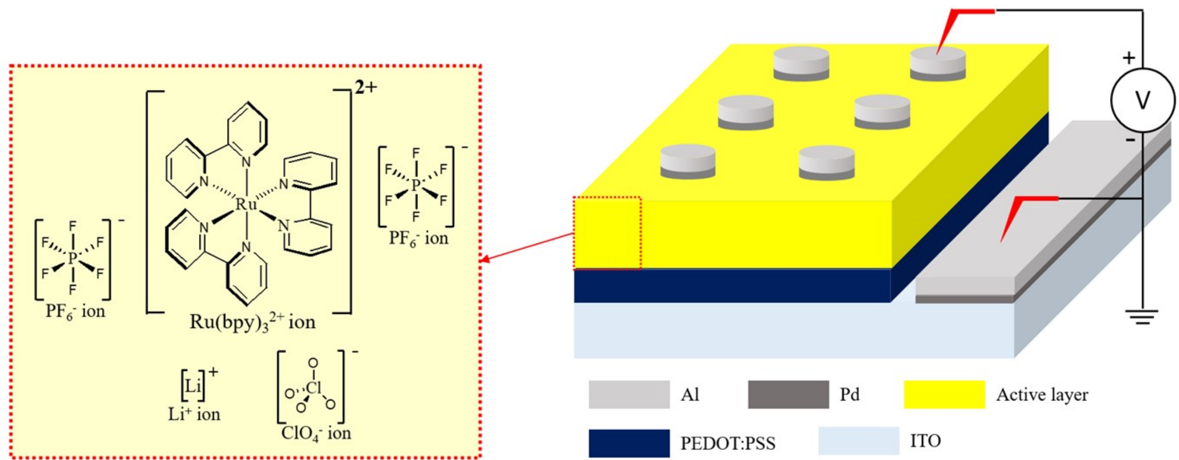

Fig. S1. Schematic structure of an OMIEC memristor device. The active layer consists of $Ru(bpy)_3^{2+}$ ions and PF_6^- ions with different concentrations of Li^+ ions and ClO_4^- ions

Equivalent Circuit Model.

The equivalent circuit model was modified and employed for our memristor devices in Fig. 3c [1–3]. The selected equivalent circuit includes a parallel circuit which consists of total electrical resistance of active layer (R_E), a constant phase element of geometric capacitance (CPE_{GEO}), capacitors of the electric double layers (EDLs) at the anode and cathode (C_{EDL1} and C_{EDL2}), resistances of the EDLs (R_{EDL1} and R_{EDL2}), and bulk ionic resistance of active layer (R_{ions}). This parallel circuit is connected with all external resistance (R_{EXT}) in series.

Constant phase element (CPE) was used because it is a model of an imperfect capacitor in an equivalent electrical circuit [3]. The impedance of the CPE can be described by the function

$$Z_{CPE} = \frac{1}{Q(i\omega)^{\alpha}} \tag{S1}$$

where ω is the applied frequency, Q is the magnitude of 1/|Z| at ω = 1 rad/s, and α is the phase of the element. Q does not have a meaningful physical value, but Q is a capacitor or a resistor when α is 1 or 0, respectively.

Table S1.

Parameters extracted from the equivalent circuit model of OMIEC memristor devices.

	R_{EXT} (kΩ)	R_E (MΩ)	Q_{GEO} (×10^{-11})	α_{GEO}	R_{ION} (MΩ)	C_{EDL1} (nF)	R_{EDL1} (pΩ)	C_{EDL2} (nF)	R_{EDL2} (pΩ)
Device-P	40	233	4.6	0.87	51.1	71	3.7	88	3.9
Device-1S	40	125	4.8	0.86	18.5	24	8.3	74	4.8
Device-2S	40	49.8	5.1	0.85	7.50	93	4.2	53	7.0

Ion concentration.

Various concentrations of $LiClO_4$ salt were added into $Ru(bpy)_3(PF_6)_2$ for tuning ion conductivity in an active layer of the OMIEC device. Fig. S2 indicated 2 wt% of salt additive have the highest ion conductivity in $Ru(bpy)_3(PF_6)_2$, and the device demonstrated similar timescales of short-term plasticity properties with biological synapse. The ion conductivity increases until 2 wt% of $LiClO_4$ because the low conductivity of $Ru(bpy)_3^{2+}$ cation can be compensated by adding Li^+ ions that are smaller in their size and thus have higher mobility than the $Ru(bpy)_3^{2+}$ ions. However, ion conductivity decreases higher than 2 wt% of $LiClO_4$, and the ion conductivity with a high (≥ 4 wt%) concentration of $LiClO_4$ showed similar or lower ion conductivity than pure $Ru(bpy)_3(PF_6)_2$ device. This showed the high concentration of $LiClO_4$ salts scatter and interrupt ion transport, leading to decrease the ion conductivity in our OMIEC memristor. A similar phenomenon can be found in the reference.[2]

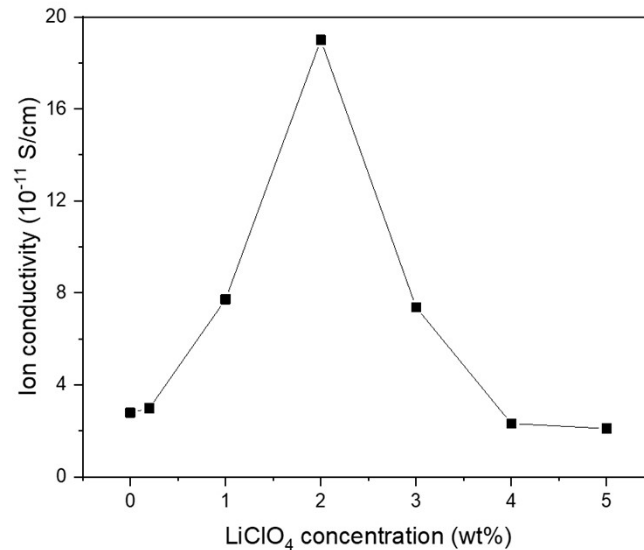

Fig. S2. Ion conductivity versus salt concentration data.

Pinched memristor hysteresis behavior.

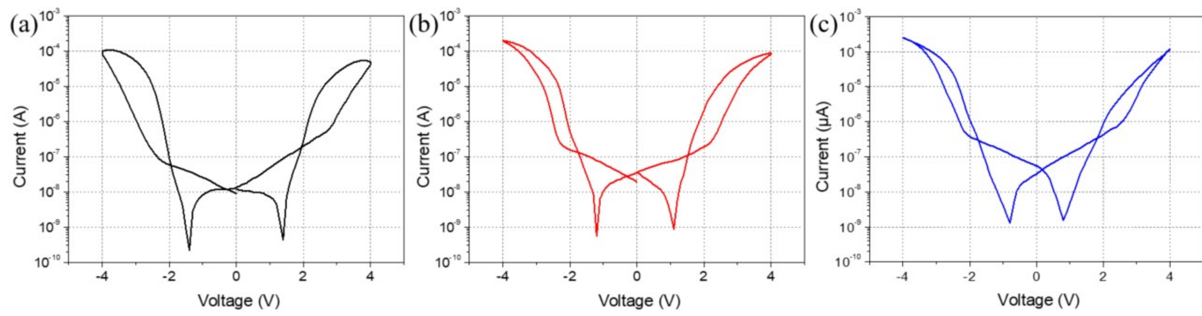

Fig. S3. Current versus voltage curves in semi-log scales of (a) Device-P, (b) Device-1S, and (c) Device-2S.

Turn-on time and relaxation time.

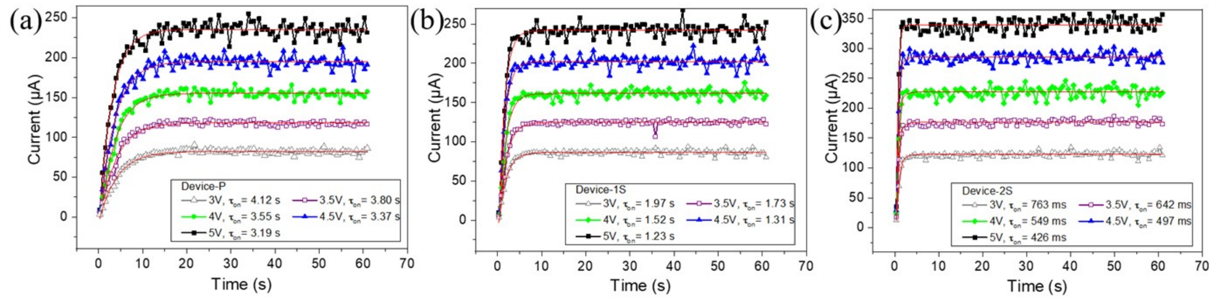

Fig. S4. The time-dependent current spectra for turn-on time of (a) Device-P, (b) Device-1S, and (c) Device-2S by varying the applied voltage from 3 to 5 V as indicated. The acquired data were fitted to Equation (1) as illustrated with solid red lines.

Table S2.

Measured turn-on time values by conducting on 10 virgin devices (3.5 V) and their average,

	Device #1 (s)	Device #2 (s)	Device #3 (s)	Device #4 (s)	Device #5 (s)	Device #6 (s)	Device #7 (s)	Device #8 (s)	Device #9 (s)	Device #10 (s)	Average (s)	Standard deviation (s)
Device-P	3.8	4.1	3.9	4.0	3.4	3.8	3.7	3.5	3.9	3.8	3.8	0.21
Device-1S	1.7	1.3	2.0	2.2	1.8	1.5	1.7	1.7	1.5	1.9	1.7	0.26
Device-2S	0.64	0.49	0.74	0.66	0.71	0.52	0.58	0.62	0.79	0.6	0.64	0.09

standard deviation.

Table S3.

Measured stabilized current values by conducting on 10 virgin devices (3.5 V) and their

	Device #1 (μA)	Device #2 (μA)	Device #3 (μA)	Device #4 (μA)	Device #5 (μA)	Device #6 (μA)	Device #7 (μA)	Device #8 (μA)	Device #9 (μA)	Device #10 (μA)	Average (μA)	Standard deviation (μA)
Device-P	108	115	129	124	99	106	112	130	124	119	117	10.3
Device-1S	128	141	112	135	125	117	137	124	128	131	128	8.38
Device-2S	0.64	0.49	0.74	0.66	0.71	0.52	0.58	0.62	0.79	0.6	178	10.4

average, standard deviation.

Table S4.

Measured relaxation time values by conducting on 10 virgin devices (1.5 V) and their average, standard deviation.

	Device #1 (s)	Device #2 (s)	Device #3 (s)	Device #4 (s)	Device #5 (s)	Device #6 (s)	Device #7 (s)	Device #8 (s)	Device #9 (s)	Device #10 (s)	Average (s)	Standard deviation (s)
Device-P	3.5	2.8	3.3	4.3	4.0	3.5	2.9	3.2	3.7	3.8	3.5	0.47
Device-1S	1.7	1.2	1.7	2.3	1.9	2.6	2.0	1.3	1.1	1.5	1.7	0.48
Device-2S	0.81	0.72	0.77	0.80	0.91	0.88	0.87	0.82	0.79	0.75	0.81	0.06

Table S5.

Measured stabilized current values by conducting on 10 virgin devices (1.5 V) and their

	Device #1 (μA)	Device #2 (μA)	Device #3 (μA)	Device #4 (μA)	Device #5 (μA)	Device #6 (μA)	Device #7 (μA)	Device #8 (μA)	Device #9 (μA)	Device #10 (μA)	Average (μA)	Standard deviation (μA)
Device-P	1.34	1.28	1.23	1.11	1.17	1.31	1.26	1.07	1.29	1.37	1.24	0.10
Device-1S	3.01	1.91	2.99	3.37	2.48	2.43	2.85	3.13	2.77	2.59	2.75	0.42
Device-2S	4.44	5.12	5.61	4.03	3.87	6.02	4.79	4.63	5.75	5.12	4.94	0.72

average, standard deviation.

Paired-pulse facilitation.

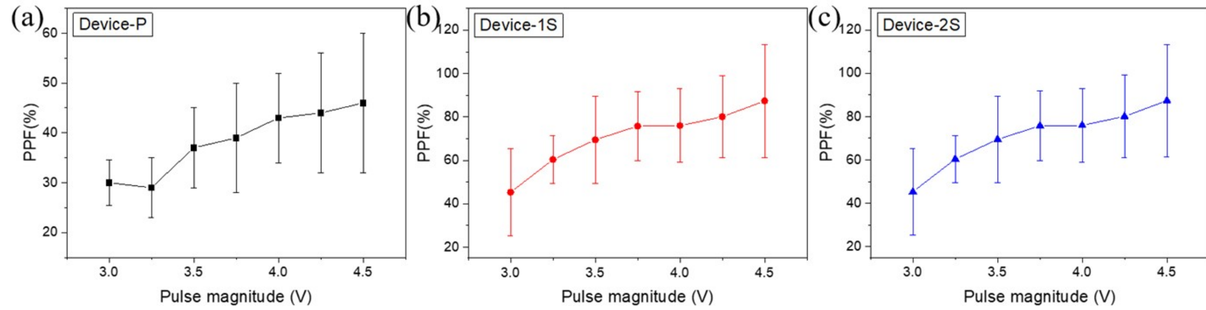

Fig. S5. PPF data and its statistical distribution as a function of the pulse magnitude with fixed pulse interval and duration at 50 ms and 100 ms, respectively, for (a) Device-P (black square), (b) Device-1S (red circle), and (c) Device-2S (blue triangle).

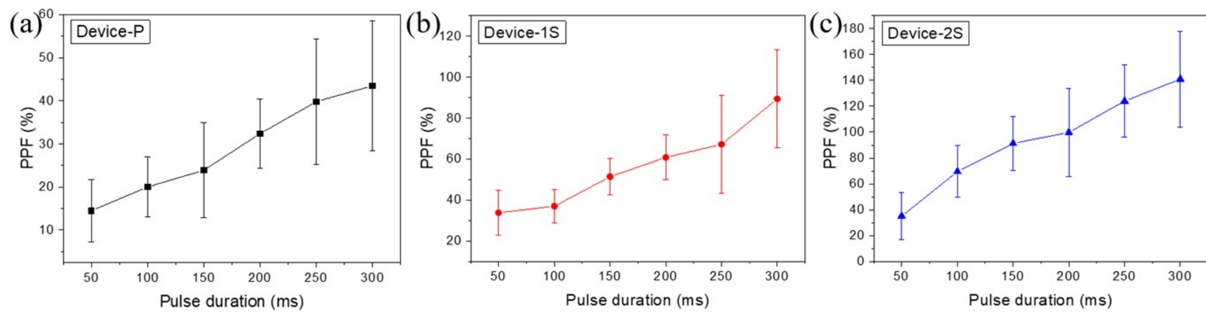

Fig. S6. PPF data and its statistical distribution as a function of the pulse duration with fixed pulse interval and magnitude at 50 ms and 3.5 V, respectively, for (a) Device-P (black square), (b) Device-1S (red circle), and (c) Device-2S (blue triangle).

VM model and fitting data.

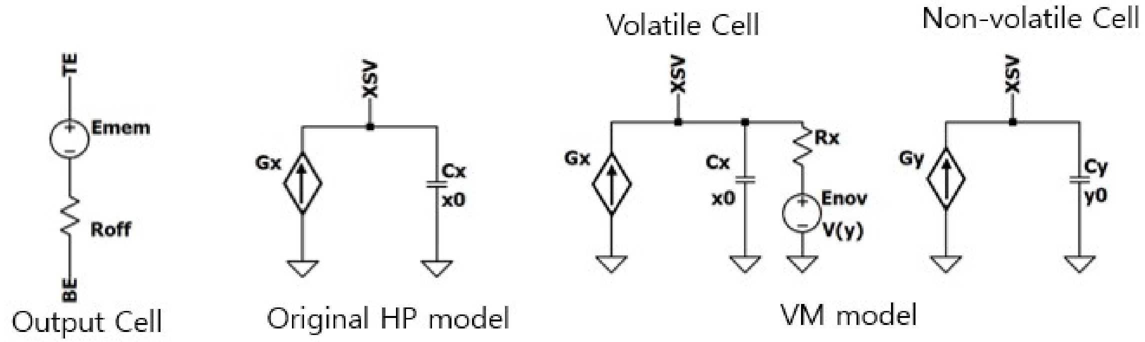

Fig. S7. Circuit schemes of the VM model.

The volatile memory model (VM model) was implemented by adding volatile properties to the HP model. The overall structure consists of a high resistance state (R_{off}) and a low resistance state (R_{on}).

$$R_{mem}(x) = (R_{on} - R_{off})x + R_{off} = \frac{v}{I_{mem}},\ 0 < x < 1$$

where R_{mem} is the total resistance of the device, V is an applied voltage, and I_{mem} is the current flow through the memristor. x is a state variable suggested by Leon Chua, which depends on the voltage applied to the device, determined by[4];

$$\frac{dx(t)}{dt} = \mu_v \frac{R_{on}}{D} I(t) f(x)$$

where μ_v is dopant mobility, D is the thickness of the insulator between two electrodes, and f(x) is the window function proposed to solve the boundary condition issues.

In the VM model, a volatile cell part is added to recover the resistance of the device to its original state when the voltage is not applied.

$$x_0 = y_0 = \frac{R_{off} - R_{init}}{R_{off} - R_{on}}$$

$$Volatile\ Cell: C_x \frac{dx}{dt} = -\frac{x-y}{R_x} + I_0(x)$$

$$Non-volatile\ Cell: C_y \frac{dy}{dt} = I_0(y)$$

$$I_0(h) = \frac{I_{mem} \cdot u_v \cdot R_{on} \cdot f(h)}{D^2}$$

Here, we use the Joglekar function as a window function, which is given by;

$$f(h) = 1 - (2x - 1)^{2p}$$

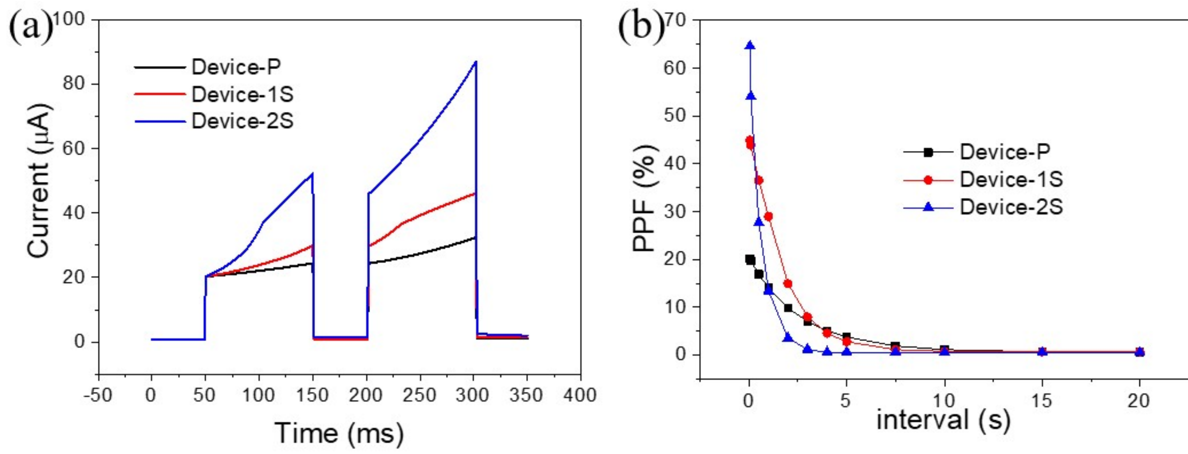

Fig. S8. Volatile model fitting result; (a) 50 ms interval PPF (b) tuning pulse interval

ECM device data and Yakopcic model

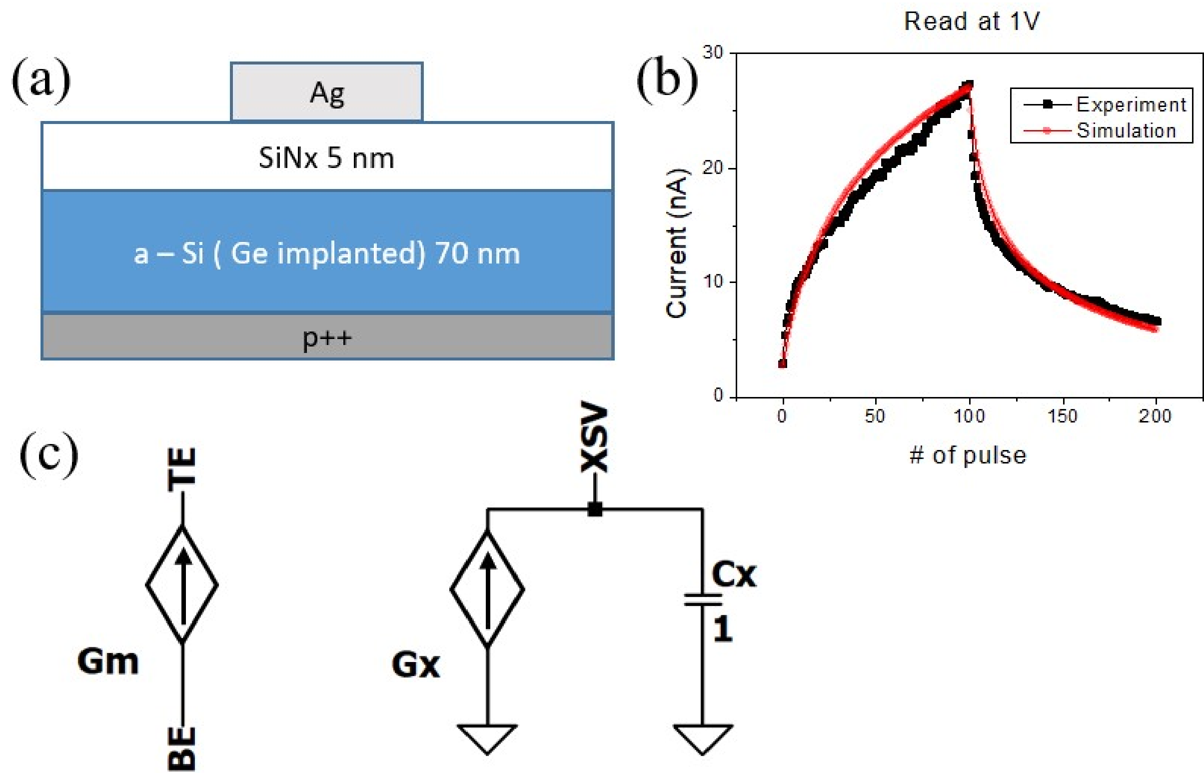

Fig. S9. (a) Schematic structure and (b) potentiation/depression test (PD test) and simulation result of the ECM device. (c) Circuit schemes of Yakopcic memristor model.

As a non-volatile device, we used Ag / SiNx / Ge implanted a-Si / p-Si ECM device (Fig. S8a), deposited a-Si with low-pressure chemical vapor deposition (LPCVD), SiNx with plasma-enhanced chemical vapor deposition (PECVD), Ag with a thermal evaporator, and implanted Ge with a 400-kV ion implanter. For measuring electrical characteristics of the device, a voltage is applied to Ag top electrode, and the low-resistance p-Si is grounded. The filament is formed at a positive voltage, lowering the resistance (set), and then ruptured at a negative voltage (reset). At the PD test, the set pulse condition is 12 V with 100 μs, and the reset pulse condition is -8 V with 100 μs (Fig. S8b). The resistance of the device is about 4 GΩ, but in the simulation, it is lowered to about 100 KΩ because the resistance should be lower than that of the OMIEC memristor.

Yakopcic memristor model introduced threshold voltage effect in the metal-insulator-metal structure.

$$I_{Gm}(t) = \begin{cases} a_1 x(t) \sinh(bV(t)), V(t) \geq 0 \\ a_2 x(t) \sinh(bV(t)), V(t) < 0 \end{cases}$$

$$I_{Gx}(t) = g(V(t)) f(V(t), x(t))$$

State variable $x(t)$ is;

$$x(t) = \int_0^t i(t) dt$$

The function $g(V(t))$ presents the threshold voltage, and $f(V(t), x(t))$ represents the change of the state variable at the boundary.

$$g(V(t)) = \begin{cases} A_p\left(e^{V(t)} - e^{V_p}\right), & V(t) > V_p \\ -A_n\left(e^{-V(t)} - e^{V_n}\right), & V(t) < -V_n \\ 0, & -V_n \leq V(t) \leq V_p \end{cases}$$

$$f(x) = \begin{cases} e^{-\alpha_p (x - x_p)} \omega_p, & x \geq x_p \\ 1, & x < x_p \end{cases}, \quad \omega_p = \frac{x_p - x}{1 - x_p} + 1$$

$$f(x) = \begin{cases} e^{\alpha_n (x + x_n - 1)} \omega_n, & x \geq x_p \\ 1, & x < x_p \end{cases}, \quad \omega_n = \frac{x}{1 - x_n}$$

where V_p, V_n is the threshold voltage, a_1, a_2, b, A_p, A_n, α_p, α_n, x_p, and x_n are fitting parameters.

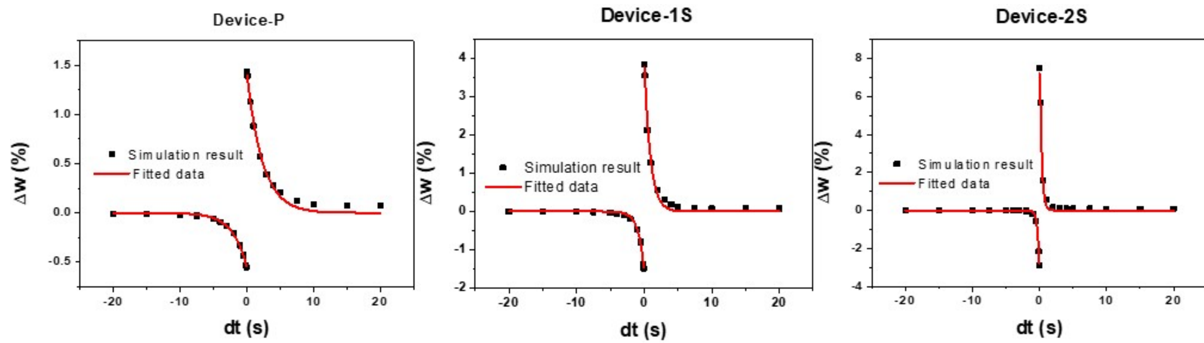

Fig. S10. STDP simulation and fitting result; as the salt concentration increases, the maximum value of Δw increases, and the value of τ_{STDP} decreases.

Reference

[1] A. Munar, A. Sandström, S. Tang, L. Edman, Shedding Light on the Operation of Polymer Light-Emitting Electrochemical Cells Using Impedance Spectroscopy, Adv. Funct. Mater. 22 (2012) 1511–1517. https://doi.org/10.1002/adfm.201102687.
[2] Discerning the Impact of a Lithium Salt Additive in Thin-Film Light-Emitting Electrochemical Cells with Electrochemical Impedance Spectroscopy | Langmuir, (n.d.). https://pubs.acs.org/doi/abs/10.1021/acs.langmuir.6b02415 (accessed January 16, 2021).
[3] S.B. Meier, D. Hartmann, A. Winnacker, W. Sarfert, The dynamic behavior of thin-film ionic transition metal complex-based light-emitting electrochemical cells, J. Appl. Phys. 116 (2014) 104504. https://doi.org/10.1063/1.4895060.
[4] D.B. Strukov, G.S. Snider, D.R. Stewart, R.S. Williams, The missing memristor found, Nature. 453 (2008) 80–83. https://doi.org/10.1038/nature06932.